Micron 190 (2025) 103775

Contents lists available at ScienceDirect

Micron

journal homepage: www.elsevier.com/locate/micron

Direct synthesis of multilayer graphene on a microscale ridge-patterned copper substrate

NaHyeon Hong [a,b,1], Minyoung Lee [a,b,1], Sungsu Kang [a,b], Jungwon Park [a,b,c,d,*]

[a] School of Chemical and Biological Engineering, and Institute of Chemical Processes, Seoul National University, Seoul 08826, Republic of Korea
[b] Center for Nanoparticle Research, Institute for Basic Science (IBS), Seoul National University, Seoul 08826, Republic of Korea
[c] Advanced Institute of Convergence Technology, Seoul National University, Suwon 16229, Republic of Korea
[d] Institute of Engineering Research, College of Engineering, Seoul National University, Seoul 08826, Republic of Korea

ARTICLE INFO

Keywords:
Copper
Photolithography
Patterning
Graphene
Epitaxial
Synthesis

ABSTRACT

Graphene's exceptional physical properties, such as high thermal conductivity and mechanical strength, have attracted significant interest for its integration in transistors and thermal interface materials. While achieving various conformations of graphene is desirable for such applications, synthesizing graphene with target conformations remains a challenge. In this work, we present a method for synthesizing multilayer graphene with ridged conformations, using a microscale ridge-patterned copper (Cu) layer that was epitaxially deposited on a sapphire substrate. The Cu layer, patterned with channels using photolithography, guides the graphene growth to conform to the ridged structure of the Cu substrate. Uniform ridged multilayer graphene is grown on the Cu substrate, and can be transferred to transmission electron microscope (TEM) grids for observation. This method offers the potential for the controlled formation of ridge patterns in graphene and could be extended to synthesizing graphene with tunable conformations for applications in graphene-based devices, electrodes, or graphene grids for graphene liquid cells and cryogenic electron microscopy for high-throughput imaging.

1. Introduction

Graphene, a two-dimensional material consisting of sp^2 carbon atoms arranged in a honeycomb lattice (Lee et al., 2017) exhibits exceptional physical properties including outstanding mechanical robustness (Novoselov et al., 2012), high thermal conductivity (Balandin et al., 2008), large specific surface area (Stoller et al., 2008), optical transmittance (Nair et al., 2008), and Young's modulus (Lee et al., 2008). Graphene is an attractive material for a wide range of applications, such as in electronic devices, catalysts, and sensors. For instance, graphene can be effectively integrated into organic field-effect transistors (OFETs) (Pang et al., 2009) and optoelectronic devices such as light-emitting diodes (LEDs) (Jo et al., 2010; Hong et al., 2023), where its superior optical transparency and mechanical strength significantly enhance device performance, durability, and efficiency (Kim et al., 2023).

Due to the versatility of graphene, significant efforts have been made to produce graphene optimized for various specific purposes. One widely known method for obtaining graphene is the exfoliation of its layers from graphite, referred to as the "scotch tape" technique, first introduced by Novoselov et al. (2004). However, for scalable graphene production, chemical vapor deposition (CVD) has emerged as a viable alternative, which utilizes the decomposition of carbon precursors and enables the controlled synthesis of large-area graphene on substrates such as copper (Cu) foils (Yang et al., 2019). CVD allows for precise control over the quality and the number of layers of graphene, facilitating its integration into various devices (Zhang et al., 2013).

Beyond large-scale production, controlling the conformations and patterns of graphene at the micrometer scale is gaining interest. Mechanical deformation (Shen et al., 2014) or geometrical changes (Zhang and Li, 2010) in graphene affect its conformation which give rise to unique physical and electronic properties (Onur et al., 2024; Kang et al., 2018; Deng and Berry, 2016). On another note, controlling the conformation of graphene is also attractive for use in electron microscopy

* Corresponding author at: School of Chemical and Biological Engineering, and Institute of Chemical Processes, Seoul National University, Seoul 08826, Republic of Korea.
E-mail address: jungwonpark@snu.ac.kr (J. Park).
[1] Equal contribution.

https://doi.org/10.1016/j.micron.2024.103775
Received 30 September 2024; Received in revised form 1 December 2024; Accepted 20 December 2024
Available online 23 December 2024

(EM), particularly in cryo-EM and liquid-phase EM, where graphene grids are used (Kang et al., 2021; Chen et al., 2020; Yuk et al., 2012; Zheng et al., 2023). For example, in liquid-phase EM, stable liquid encapsulation within the graphene is more likely to be successful in regions with folds (van Deursen et al., 2020; Bae et al., 2022). As such, being able to control the formation of different conformations of graphene is highly desirable. However, conventional methods like the 'scotch tape' technique or chemical vapor deposition (CVD) offer limited control over graphene's shape and conformation. This is primarily because the conformation of graphene is determined by the properties of the substrate from which it is synthesized and transferred. Many conventional substrates, such as polycrystalline copper foils, tend to have inherent roughness, as well as a random variation of domains with different crystalline orientations which have different thermal expansion coefficients (Yao et al., 2022). These factors significantly influence the number of layers and the morphology of graphene synthesized (Wood et al., 2011). As a result, the ability to control graphene's shape and conformation is restricted, which poses challenges for its integration into semiconductor devices where precise structural control is critical (Feng et al., 2012).

In addressing these limitations, approaches for engineering the substrate have provided advantages for controlling the conformational properties of graphene that is synthesized. For instance, with the aim of synthesizing high quality, flat graphene with low defect density, a modified substrate made of c-axis α-Al_2O_3 wafer with epitaxially grown, flat and single-crystalline Cu(111) was used. This method uses the minimal thermal expansion mismatch between Cu(111) and graphene, which promotes uniform growth while avoiding the inherent roughness of the conventional Cu foil which may introduce undesired conformational heterogeneities in the graphene (Deng et al., 2017). Additionally, it was observed that defect lines of metal substrates (Deng et. al., 2016) promote the formation of microscale graphene wrinkles. An earlier study has leveraged this substrate-dependent property of graphene synthesis, revealing that with patterned curvatures on the Cu substrate, the graphene synthesized had more folds along the directions of the curves (Kim et al., 2011). Given that graphene's conformation is highly dependent on the properties of the substrate it is synthesized on, the controlled modification of the substrate provides the possibility of producing graphene with tailored structures.

In this study, we present a method for synthesizing microscale ridged graphene that conforms to the shape of a patterned Cu substrate. Channel-type ridge shapes are patterned on copper-deposited sapphire

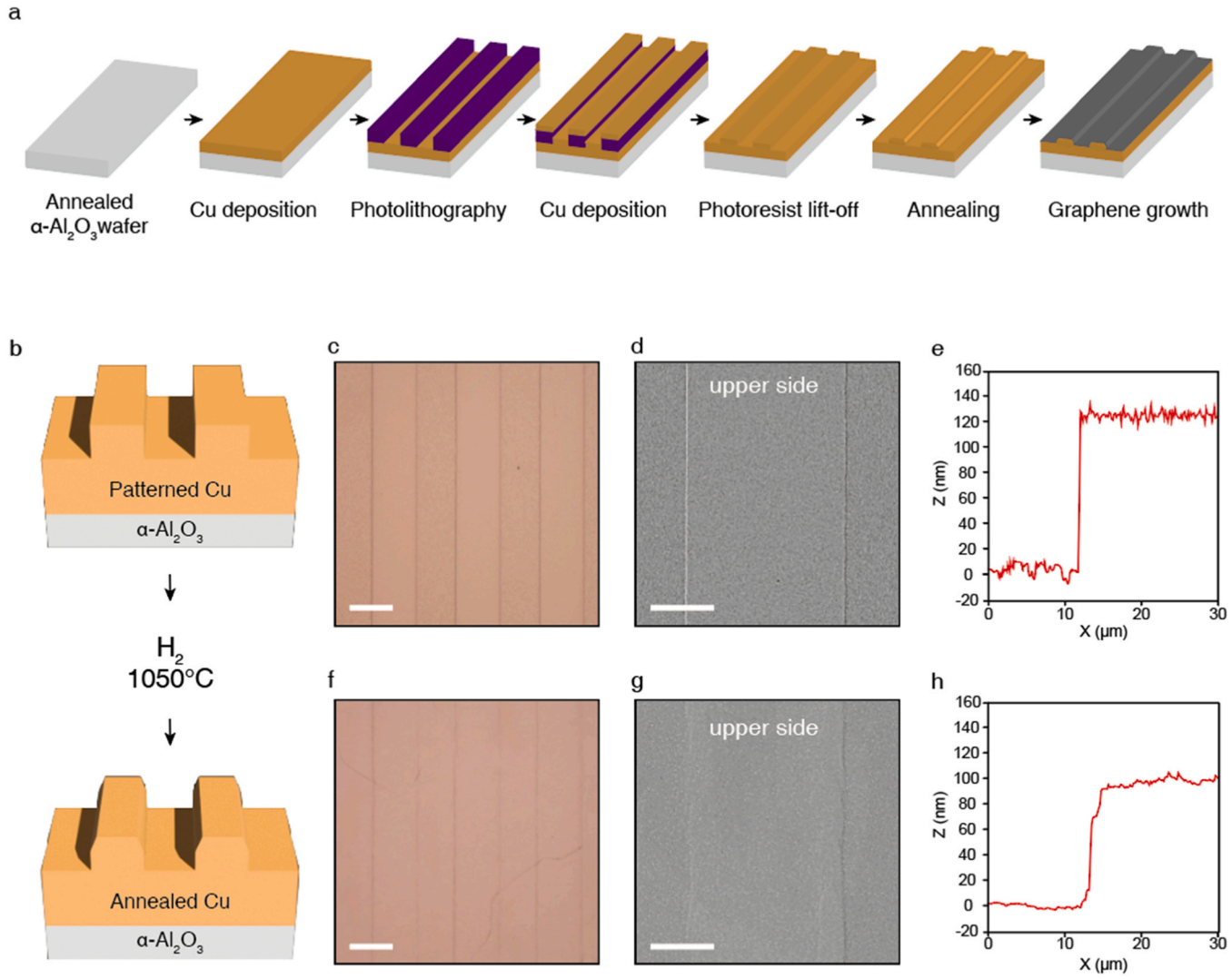

Fig. 1. Patterned substrate fabricated for synthesizing ridged graphene (a) Schematic of the fabrication of patterned graphene. Cu is patterned with 100 nm height and 50 μm width using photolithography. Then, Cu is deposited, and the patterned photoresist beneath the Cu film is lifted off. The substrate is then annealed. During the annealing process, the ridges on the substrate are smoothened. (b) Schematic of patterned substrate before and after annealing which illustrates how the topography of the ridge edge changes. (c) OM, (d) SEM images, and (e) height profile from AFM at the Cu ridge before the annealing process. (f) OM, (g) SEM images, and (h) height profile from AFM at the Cu ridge after the annealing process. Scale bars are 50 μm for OM images and 20 μm for SEM images.

wafers using photolithography. During annealing, the substrate forms Cu(111) planes aligned in the out-of-plane direction through epitaxial growth with the sapphire. Multilayer ridged graphene is then synthesized via chemical vapor deposition (CVD), achieving uniform thickness across the entire wafer presumably due to the epitaxial relationship between Cu(111) and graphene. Finally, the graphene can be transferred to a TEM grid for observation, where some of the ridge shapes remain preserved. This approach provides a method for producing graphene with three dimensional ridged patterns in the micrometer scale, making it applicable to numerous industry fields such as semiconductor, various electrical devices, and analytical techniques in nanoscience.

2. Results and discussion

2.1. Preparation of microscale-patterned Cu layer for conformation-controlled graphene synthesis

In our approach to synthesize ridge-patterned graphene, we have employed photolithography, Cu deposition, and a lift-off process to produce a patterned substrate for graphene growth. Fig. 1a illustrates the schematic overview of the method, with detailed experimental conditions described in the Methods section. A Cu layer with a thickness of 500 nm was deposited on a c-plane sapphire (α-Al_2O_3) wafer using thermal evaporation. Photolithography was then performed to pattern the Cu layer. A photomask consisting of channel-type patterns with 50 μm ridges was designed for selective exposure of UV through the mask. The unexposed PR was removed with a developer. Additional Cu was deposited on the substrate, after which the remaining PR was removed and the Cu on top of the PR was lifted off, resulting in a Cu substrate targeting channels of 50 μm width and 100 nm height.

The ridge-patterned substrate was then annealed in a CVD chamber under an Ar and H_2 environment at 1050 °C to allow recrystallization of the Cu substrate (Fig. 1b). This recrystallization process is known to produce larger Cu grains on the substrate, which minimizes grain boundaries and enhances the quality of the Cu as a catalyst for graphene growth (Li et al., 2021; Ding et al., 2023; Long et al., 2021). Fig. 1c–e show results of the ridge-patterned Cu substrate prior to annealing. The optical microscopy (OM) image (Fig. 1c) and scanning electron

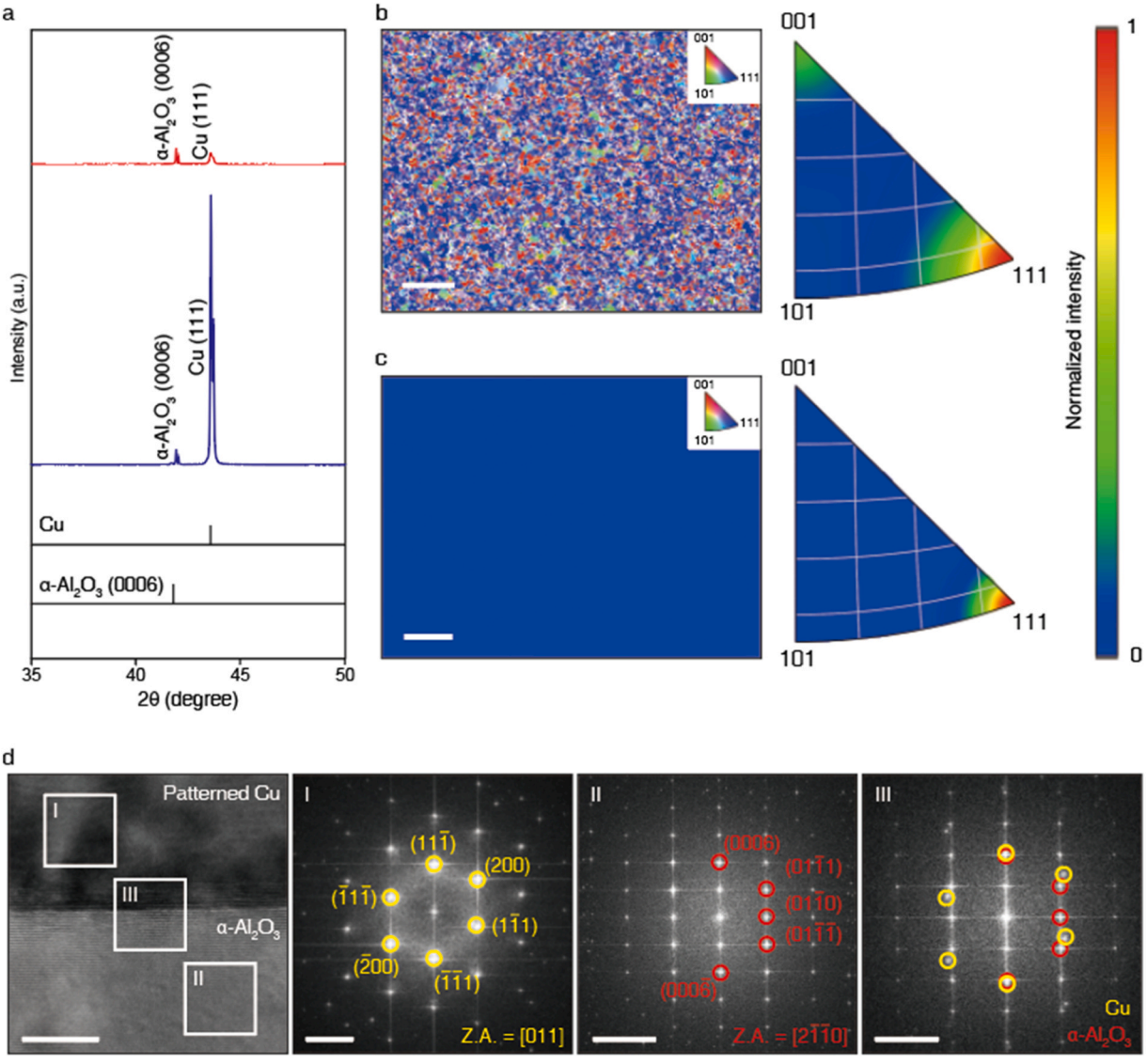

Fig. 2. Epitaxial growth of patterned Cu on sapphire by annealing (a) XRD of Cu/sapphire before (blue line) and after (red line) annealing and XRD simulated results for comparison. A slight split in the Cu(111) peak is attributed to K-alpha splitting. (b,c) EBSD maps (left) and inverse pole figures (right) of patterned Cu substrate in the out-of-plane direction before (b) annealing and (c) after annealing. The scale bar is 10 μm. (d) cross-sectional TEM image of Cu/α-Al_2O_3, fast Fourier Transforms of indicated spots in the image, representing regions of the (I) α-Al_2O_3(0006), (II) Cu(111), (III) α-Al_2O_3 and Cu combined. The scale bar of the TEM image is 10 nm, and FFTs are 5 nm^{-1}.

microscopy (SEM) image (Fig. 1d) confirm that the channels have been successfully patterned and the height plot from atomic force microscopy (AFM) data (Fig. 1e) shows a sharply defined step edge with a ridge height of approximately 120 nm. During SEM image acquisition (Fig. 1d), the sample was tilted at 40° to enhance the visibility of the step edge, which was clearly observed due to the brighter contrast along the boundary. With the electron beam directed from the left in the SEM image, we identified the area between the two edge lines as the upper side of the step, based on the contrast differences along the edge. The upper side of the step is indicated in Fig. 1d. This analysis confirmed that the contrast differences observed in the OM image (Fig. 1a) were due to the height variation between the ridges in the structure. After the substrate was annealed, the OM image (Fig. 1f) and SEM image (Fig. 1g) demonstrates that the patterned structure exhibits smoothened step edges, which are shown by ridge boundaries that are less defined, but still maintains the three-dimensional step structure. The smoothening of the edges is also demonstrated by the shape of the AFM profile, in which the edge areas exhibit a more gradual increase (Fig. 1h). The smoothening suggests a structural change in the Cu layer after annealing. Notably, the AFM profile also reveals that the height of the ridge has decreased to 98 nm, but also indicates that the patterned ridge is still maintained even after the high-temperature annealing process.

2.2. Epitaxial growth of the patterned Cu film on sapphire

Next, we investigate the structural changes that occur after the annealing of the deposited Cu on α-Al_2O_3, which will serve as the substrate that controls graphene growth. Fig. 2a presents the X-ray diffraction (XRD) profiles of patterned Cu deposited on sapphire wafer with the red plot representing the sample before annealing process and the blue plot representing the sample after the annealing process. Both profiles exhibit reflections from α-Al_2O_3(0006) from the sapphire wafer and Cu(111) from the Cu layer, as confirmed by comparing the reflections to peak positions of simulated XRD. The peaks were normalized with the intensity of the α-Al_2O_3(0006) peaks, which arise from the single-crystalline sapphire wafer present in the samples both before and after annealing. Cu(111) and α-Al_2O_3(0006) peaks were detected in both samples, but a significant increase in the height of the Cu(111) peak after annealing relative to the sample before annealing suggests that the majority of the Cu film exhibits out-of-plane orientation of Cu(111) after annealing. These results are consistent with previous reports on the orientation preference of Cu(111) along the axis normal to α-Al_2O_3(0001) (Ma et al., 2018; Miller et al., 2012). The orientation preference achieved by annealing is further demonstrated by electron backscatter diffraction (EBSD) maps obtained from the out-of-plane direction that demonstrate the change in crystallinity after annealing (Fig. 2b and c). Before annealing, the EBSD map exhibits polycrystallinity of the Cu film, shown by randomly distributed crystal planes of Cu, in which each color represents a different crystal domain (Fig. 2b). The inverse pole figure located in the right side of the EBSD map in Fig. 2b shows that while the majority of the domains within the observed area is the Cu(111) domain, a significant portion consists of the Cu(001) domain. After annealing, the EBSD map (Fig. 2c) exhibits a uniform blue color, indicating that the majority of the crystal domains has been aligned with Cu(111) in the out-of-plane direction. The inverse pole figure in the right of Fig. 2c for the annealed sample also indicates that the viewing area exhibits only Cu(111) in the direction perpendicular to the substrate, which is likely due to the epitaxial relationship between Cu(111) and the c-plane in the underlying α-Al_2O_3 substrate. The epitaxial relationship was further observed through cross-sectional, high resolution transmission electron microscopy (HRTEM) imaging of the Cu on sapphire interface, which was sampled using focused ion beam (FIB) as outlined in the Methods section. The HRTEM cross sectional image shows that the Cu film is located on the top of the α-Al_2O_3 (Fig. 2d). The Fast Fourier Transforms (FFTs) for the HRTEM images from each designated area marked with white boxes, labeled with I, II and III in regions of Cu, α-Al_2O_3, and the Cu/α-Al_2O_3 interface, respectively. The FFT pattern obtained from the Cu film (box I) confirms the presence of {111} and {002} planes, indicating that the zone axis is [011]. The FFT pattern of the sapphire wafer (box II) shows the {0006} and $\{01\bar{1}0\}$ planes, which are the Miller-Bravais indices of hexagonal α-Al_2O_3 at the zone axis of $[2\bar{1}\bar{1}0]$. Additionally, when the FFT is applied across the combined region (box III), the FFT shows two sets of peaks that arise from both zone axes. Notably, in the FFT from box III, the Cu $(1\bar{1}0)$ plane and the α-Al_2O_3(0006) plane are aligned in the same direction within the observed area. The results from cross-sectional HRTEM demonstrate that the patterned Cu film on the substrate has been crystallized so that the Cu(111) is aligned in the perpendicular orientation with respect to the substrate, due to its epitaxial relationship with the α-Al_2O_3(0006) plane. These results indicate that the majority of the Cu film in the annealed patterned substrate has Cu(111) oriented towards the out-of-plane direction, which will serve as the surface for synthesis of graphene using CVD.

2.3. Uniform multilayer graphene growth on the patterned Cu substrate

Multilayer graphene was grown on the annealed substrate in the CVD chamber using methane gas as the graphene precursor. After graphene synthesis, Raman spectroscopy was conducted for the graphene on the prepared substrate in the areas designated by white boxes numbered 1–5 on the image of a wafer (Fig. 3a), and the enlarged OM image of the box numbered 5 in Fig. 3a depicts a close-up region of the ridge edge (Fig. 3b). To evaluate the uniformity of graphene on both the top and the bottom of the ridges, Raman spectra obtained at the upper (red box in Fig. 3b) and lower (blue box in Fig. 3b) areas of the ridges in five different regions of the substrate are presented in Fig. 3c and Fig. 3d, respectively. All the Raman spectra obtained at marked regions of the wafer display the characteristic G and 2D peaks associated with pristine graphene with little defects. The peak positions of the G and 2D peaks remain consistent for all the spectra acquired at different regions, confirming the uniform properties of the synthesized graphene across the substrate, as well as on both the top and bottom of the ridges. The ratio of intensities of the 2D and G peaks provides insight into the number of graphene layers. Fig. 3e shows the point mapping results of the Raman spectra, where I_{2D}/I_G values were extracted from spectra obtained from the point maps. This was performed for each of the areas 1–5 designated in Fig. 3a. We note that the point maps include values obtained from the top, bottom, and the edges of the ridges which are marked by white dashed lines. The point maps mostly exhibit a uniform orange color within the mapping range, indicating consistent values. The average I_{2D}/I_G value for all point spectra obtained is 0.62 with a standard deviation of 0.36, a value which corresponds to few-layer graphene grown throughout the wafer. Further investigation on the graphene grown near the edge of a ridge was conducted through cross-sectional HRTEM analysis of a ridge edge site (Fig. 3f). The cross section shows the smoothened morphology of the ridge on the substrate with a ridge height of 85 nm, as expected by results in Fig. 1h. HRTEM images of designated areas marked with white boxes, labeled I, II and III are also shown in Fig. 3f. Graphene layers are visible in close proximity above the region of the Cu substrate, indicating that graphene has grown directly on the substrate. The number of graphene layers can be identified in the HRTEM image by the number of bright lines that suggest the presence of graphene layers. The cross-sectional images show that about 5–7 layers of graphene have been synthesized along the Cu step uniformly throughout the observed area. The combination of Raman spectroscopy and HRTEM analysis confirms the uniform synthesis of few-layer graphene, with a consistent layer thickness and high quality across the patterned Cu substrate, including both ridge tops, bottoms and edges.

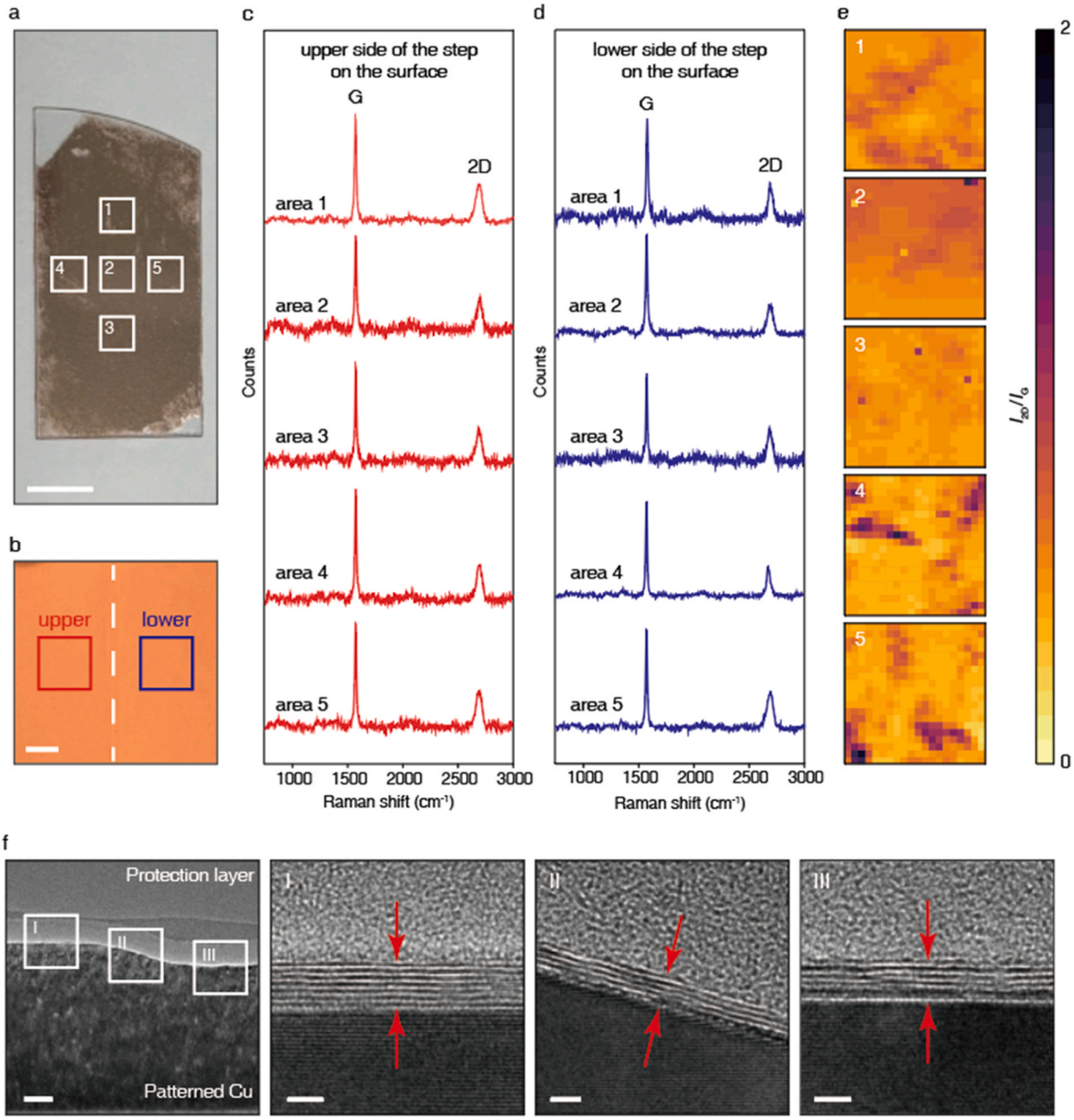

Fig. 3. Uniformity of multilayer graphene grown on the patterned substrate (a) OM image of the whole substrate with designated areas where Raman data was collected. Scale bar is 1 cm. (b) Optical image showing the enlarged region of the edge in the ridged pattern of Cu. Scale bar is 5 μm. (c) Raman spectra obtained from the upper side of the step in each of the areas 1 through 5. (d) Raman spectra obtained from the lower side of the step edge in each of the areas 1 through 5. (e) Raman mapped data of the ratio of intensities of the 2D and G peaks (I_{2D}/I_G), including the Cu step obtained from the areas indexed in OM image in (a) (Dimensions = 20 by 20, step size = 0.5 μm). (f) HRTEM images of the edges of patterned Cu, followed by the HRTEM images of graphene obtained from each region indexed by I, II and III. The scale bar is 100 nm for the first image which shows the step edge of patterned Cu and 2 nm for the following images.

2.4. Graphene transfer for free-standing characterization

The transfer process of graphene is crucial for extending its applications, as well as analyzing its free-standing properties without the influence of a supporting substrate. Our synthesized graphene was transferred to a holey-carbon Quantifoil™ TEM grid using a polymer-based method for further analysis, with detailed procedures provided in the Methods section and Fig. S1. The transferred graphene is free-standing in the regions of the holes in the TEM grid, and its image is shown in Fig. 4a. Raman analysis was performed at eight locations on the grid, as indicated in the TEM grid image (Fig. 4a), which confirms the presence of free-standing multilayer graphene. The average I_{2D}/I_G ratio for these spectra is 0.61, which is consistent with that of the ridged graphene on the Cu/α-Al_2O_3 substrate, confirming the consistency of the free-standing graphene results with the substrate-supported results as discussed earlier. Some edges of the ridges in the transferred graphene remain intact even after the transfer process, with one such edge depicted in Fig. 4c, where a folded region has been observed. The AFM image conducted with the transferred graphene on the TEM grid confirms this ridge pattern for the graphene (Fig. S2a). While the graphene was initially was synthesized on a substrate with 100 nm step heights, AFM results show that the ridge became lower but can still be maintained even after being transferred to the TEM grid, as shown in Fig. S2b. Additionally, the correlation between the ridged pattern and wrinkle formation is evident, as the direction of the ridges aligns with the orientation of the wrinkles observed in TEM, suggesting that the ridges

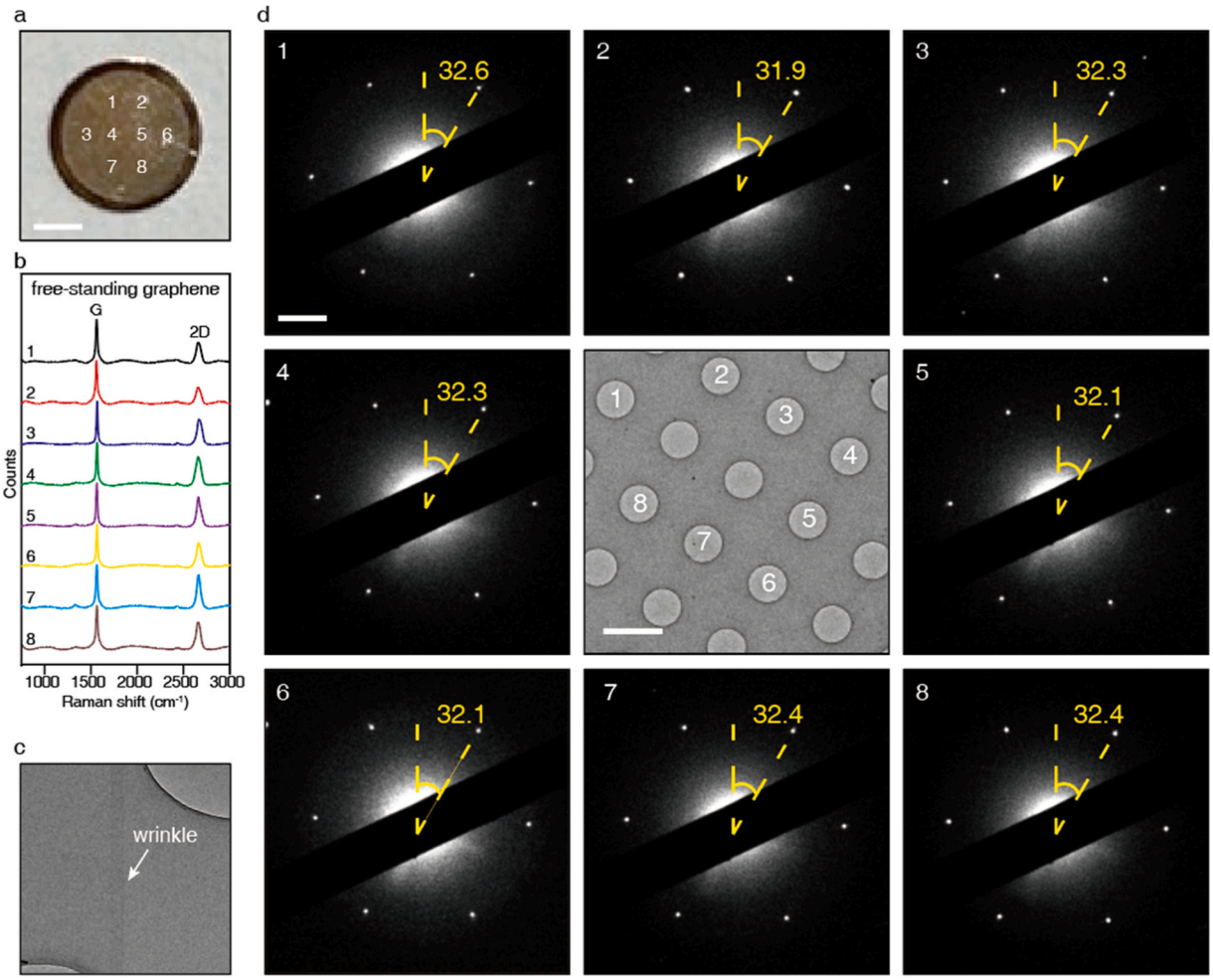

Fig. 4. Graphene transfer onto TEM grid for free-standing characterization (a) Image of a holey-carbon Quantifoil™ TEM grid. Scale bar is 1 mm. (b) Raman spectra of free-standing graphene obtained from the numbered locations in the TEM grid image in (a). (c) TEM image of the step edge of the transferred graphene, manifested as a wrinkle labeled in white. (d) TEM image of the holes in the TEM grid (center) and SAED patterns obtained from the numbered positions of the center image (surrounding images). The angles between the vertical line and a designated peak at the top right are measured for each SAED pattern and are labeled in yellow. Scale bar of the center image is 2 μm and those for SAED patterns are 2 nm^{-1}.

play a critical role in guiding wrinkle formation (Supplementary Text 1). Fig. 4d exhibits SAED patterns from eight different holes of the TEM grid obtained from the regions labeled from 1 to 8 in the center image. Each SAED pattern shows the hexagonal pattern characteristic of the crystalline structure of graphene. Additionally, the angles of the hexagonal patterns can provide insight into the orientations of the graphene domains. In each SAED pattern, the angles of a designated peak with respect to the vertical line are shown to be consistent. This demonstrates that the transferred graphene maintains crystallographic alignment across multiple regions of the TEM grid, which suggests that single-crystalline graphene is synthesized and transferred in scales of at least tens of micrometers. These results from graphene transfer can further be utilized for applications in producing graphene grids for cryo-EM or liquid-phase EM analysis, in which single-crystalline graphene substrates that exhibit uniform microscale properties with consistent conformational patterns are highly desirable.

3. Conclusion

We have developed a technique for synthesizing microscale-ridged graphene on a patterned Cu substrate, which was achieved by microscale patterning of the Cu film using photolithography, followed by the CVD synthesis of graphene on the fabricated substrate. The α-Al_2O_3(0001) from the wafer and the Cu(111) plane from the patterned Cu film exhibit epitaxial relationship, which enables the growth of Cu (111) along the out-of-plane direction for the majority of the substrate. With the ridge-patterned Cu serving as a catalytic layer for graphene growth, multilayer graphene with uniform thickness was directly grown on the patterned substrate. Furthermore, the multilayer graphene can be transferred onto a holey-carbon TEM grid for observation. The results pave the way for more precise production of multilayer graphene with various conformations, which holds significant potential for applications ranging from industrial fields, such as field-effect transistors (FETs), to nanoscience, such as for sample preparation in cryogenic electron microscopy or for graphene liquid cells.

CRediT authorship contribution statement

NaHyeon Hong: Writing – review & editing, Writing – original draft, Investigation, Formal analysis, Data curation, Conceptualization. **Sungsu Kang:** Writing – original draft, Methodology, Investigation. **Minyoung Lee:** Writing – review & editing, Writing – original draft, Investigation, Formal analysis, Data curation, Conceptualization. **Jungwon Park:** Writing – review & editing, Supervision, Funding acquisition.

Author contributions

N.H. and M.L. contributed equally to this work. N.H. and M.L. designed the experiment, conducted the measurement, analyzed the data and prepared the manuscript. N.H. and M.L. conducted the fabrication of the materials. S.K. performed HRTEM. M.L. and S.K. offered valuable comments and discussion on the experimental design and analyses. J.P. supervised the project and contributed to the experimental planning, data analysis and manuscript preparation.

Declaration of Competing Interests

The authors declare no competing interests.

Declaration of Competing Interest

The authors declare that they have no known competing financial interests or personal relationships that could have appeared to influence the work reported in this paper.

Acknowledgements

This work was supported by the National Research Foundation of Korea (NRF) grants funded by the Korean government (RS-2024-00421181 and RS-2023-00283902). This work was supported by the Institute for Basic Science (IBS, IBS-R006-D1). The authors acknowledge financial and technical support from the Samsung Science & Technology Foundation (SSTF-BA2302-06) for materials synthesis and characterization. The authors thank the staff of the National Center for Inter-university Research Facilities at Seoul National University for assistance with the SEM, FIB, and Cs-TEM experiments.

Appendix A. . Additional information

B. Methods

B.1. Substrate patterning and annealing

A sapphire wafer with c-axis orientation was cleaned with ethanol and acetone, followed by annealing at 1000 °C for 6 h in an air environment. Cu was deposited using a thermal evaporator to a thickness of 500 nm. For lithography, approximately 1 μm layer of ma-N 1410 negative photoresist (PR) was spin-coated, and using a Cr photomask with repeating microscale channel patterns, the PR was exposed with UV according to the channel patterns of the Cr photomask. The unexposed areas of photoresist were removed with ma-D 533/s developer solution. After that, a Cu film targeting 100 nm was deposited with a thermal evaporator. The remaining PR and the Cu film deposited on top of the PR were removed using a lift-off process with mr-REM 700 solution, which results in a ridge-patterned copper substrate. The patterned substrate was annealed in a 5:1 Ar:H_2 atmosphere for one hour at 1050 °C.

B.2. Graphene synthesis

Multilayer graphene was synthesized on the ridge-patterned Cu/Al_2O_3 substrate using chemical vapor deposition (CVD). The substrate was positioned at approximately a 30° angle inside a horizontal chamber. The chamber was maintained at atmospheric pressure, with a synthesis temperature of 1050 °C and a gas mixture ratio of Ar:H_2:CH_4 = 500:100:1. The temperature increases to 1050 °C for 1 h and anneals the substrate for 1 h in the Ar and H_2 atmosphere. After the annealing, CH_4 started to flow and was held for 20 min.

B.3. Graphene transfer to TEM grids

400 μm of 40 g/L Poly(methyl methacrylate) (PMMA) chlorobenzene was coated on the Cu/Al2O3 substrate using a spin coater. After the substrate was dried, the Cu/Al2O3 substrate was submerged into 1 M ammonium persulfate solution to dissolve the Cu film, which isolates the graphene layer combined with PMMA from the substrate. The isolated graphene were picked up using Pt loop and rinsed with deionized water before being attached to the TEM grids, which were exposed to glow discharge to make the hydrophobic surface hydrophilic. The transferred graphene on the TEM grid was heated at 40 °C to evaporate the water and then at 180 °C for 30 min for strong attachment. After the baking process, the TEM grid was submerged into acetone to dissolve the PMMA layer.

B.4. Characterization of the annealed Cu/sapphire substrate

Optical microscopy and scanning electron microscopy (GeminiSEM 560, JEOL) were used to verify the ridge shapes of the Cu/sapphire substrate. Noncontact mode atomic force microscopy (NX-10, Park systems) was used to characterize the surface profiles of the substrates. For XRD, EBSD and cross-sectional TEM, the Cu/sapphire substrate was prepared and annealed in the same way as done for graphene synthesis, and then was diced into 1 cm by 1 cm pieces for analysis. The XRD data (SmartLab, Rigaku) was obtained by securing the prepared substrate on a quartz holder. Electron backscatter diffraction (Oxford instruments) was performed with Cu phase in ND direction, and the step size is 200 nm. The cross-sectional transmission electron microscope sample was prepared by focused ion beam milling (Helios NanoLabTM 650, ThermoFisher) on a region containing the ridge and the boundary between the Cu film and the sapphire wafer. Cross-sectional TEM images were acquired with aberration-corrected TEM (ARM-200F, JEOL), operated at 200 kV. Images and selected area electron diffraction patterns for graphene transferred to the TEM grids were taken with JEM-2100F, JEOL.

B.5. Characterization of graphene

Raman spectroscopy and mapping was conducted by using a 532-nm laser source. The background of the Raman spectra that arises from the Cu film was removed using an iterative polynomial-fit background removal function.

Appendix B. Supporting information

Supplementary data associated with this article can be found in the online version at doi:10.1016/j.micron.2024.103775.

Data availability

Data will be made available on request.

References

Bae, Y., Ha, M.Y., Bang, K.-T., Yang, S., Kang, S.Y., Kim, J., Sung, J., Kang, S., Kang, D., Lee, W.B., Choi, T.L., Park, J., 2022. Conformation dynamics of single polymer strands in solution. Adv. Mat. 34, 2202353. https://doi.org/10.1002/adma.202202353.

Balandin, A.A., Ghosh, S., Bao, W., Calizo, I., Teweldebrhan, D., Miao, F., Lau, C.N., 2008. Superior thermal conductivity of single-layer graphene. Nano Lett. 8, 902–907. https://doi.org/10.1021/nl0731872.

Chen, L., Leonardi, A., Chen, J., Cao, M., Li, N., Su, D., Zhang, Q., Engel, M., Ye, X., 2020. Imaging the kinetics of anisotropic dissolution of bimetallic core-shell nanocubes using graphene liquid cells. Nat. Commun. 11, 3041. https://doi.org/10.1038/s41467-020-16645-3.

Deng, B., Pang, Z., Chen, S., Li, X., Meng, C., Li, J., Liu, M., Wu, J., Qi, Y., Dang, W., Yang, H., Zhang, Y., Zhang, J., Kang, N., Xu, H., Fu, Q., Qiu, X., Gao, P., Wei, Y., Liu, Z., Peng, H., 2017. Wrinkle-free single-crystal graphene wafer grown on strain-engineered substrates. ACS Nano 11, 12337–12345. https://doi.org/10.1021/acsnano.7b06196.

Deng, S., Berry, V., 2016. Wrinkled, rippled and crumpled graphene: an overview of formation mechanism, electronic properties, and applications. Mater. Today 19, 197–212. https://doi.org/10.1016/j.mattod.2015.10.002.

van Deursen, P.M.G., Koning, R.I., Tudor, V., Moradi, M.-A., Patterson, J.P., Kros, A., Sommerdijk, N.A.J.M., Koster, A.J., Schneider, G.F., 2020. Graphene liquid cells assembled through loop-assisted transfer method and located with correlated light-electron microscopy. Adv. Funct. Mater. 30, 1904468. https://doi.org/10.1002/adfm.201904468.

Ding, Y.P., Zhang, M., Zhou, S.Y., Fan, H.Y., Liu, S.F., Ran, C.H., Yuan, X.L., 2023. Microstructure and texture of ultra-high purity copper under changed rolling strain

paths and subsequent recrystallization annealing. Phys. Met. Metallogr. 124, 1392–1403. https://doi.org/10.1134/S0031918X22601858.
Feng, J., Li, W., Qian, X., Qi, J., Qi, L., Li, J., 2012. Patterning of graphene. Nanoscale 4, 4883–4899. https://doi.org/10.1039/c2nr30790a.
Hong, S., Hong, C., Lee, S., Jang, M., Jang, C., Lee, Y., Widiapradja, L., Park, S., Kim, K., Soo, Y., Yook, J., Im, S., 2023. Ultrafast van der Waals diode using graphene quantum capacitance and Fermi-level depinning. Sci. Adv. 9 (29). https://doi.org/10.1126/sciadv.adh9770.
Jo, G., Choe, M., Cho, C.Y., Kim, J.H., Park, W., Lee, S., Hong, W.K., Kim, T.W., Park, S.J., Hong, B.H., Kahng, Y.H., Lee, T., 2010. Large-scale patterned multi-layer graphene films as transparent conducting electrodes for GaN light-emitting diodes. Nanotechnology 21. https://doi.org/10.1088/0957-4484/21/17/175201.
Kang, P., Kim, K.-H., Park, H.-G., Nam, S., 2018. Mechanically reconfigurable architectured graphene for tunable plasmonic resonances. Light Sci. Appl. 7, 17. https://doi.org/10.1038/s41377-018-0002-4s.
Kang, S., Kim, J., Lee, M., Yu, J., Kim, J., Kang, D., Baek, H., Bae, Y., Kim, B.H., Kang, S., Shim, S., Park, S.J., Lee, W.B., Hyeon, T., Sung, J., Park, J., 2021. Real-space imaging of nanoparticle transport and interaction dynamics by graphene liquid cell TEM. Sci. Adv. 7 (49). https://doi.org/10.1126/sciadv.abi5419.
Kim, K., Lee, Z., Malone, B., Chan, K., Alemán, B., Regan, W., Gannett, W., Crommie, M., Cohen, M., Zettl, A., 2011. Multiply folded graphene. Phys. Rev. B Condens. Matter 83. https://doi.org/10.1103/PhysRevB.83.245433.
Kim, S., Jiang, S., Lee, S., 2023. Direct CVD Growth of Transferable 3D Graphene for Sensitive and Flexible SERS Sensor. J. Nanomater. 6 (13). https://doi.org/10.3390/nano13061029.
Lee, C., Wei, X., Kysar, J.W., Hone, J., 2008. Measurement of the elastic properties and intrinsic strength of monolayer graphene. Science 321, 385–388. https://doi.org/10.1126/science.1156211.
Lee, H.C., Liu, W.W., Chai, S.P., Mohamed, A.R., Aziz, A., Khe, C.S., Hidayah, N.M.S., Hashim, U., 2017. Review of the synthesis, transfer, characterization and growth mechanisms of single and multilayer graphene. RSC Adv. 7, 15644–15693. https://doi.org/10.1039/C7RA00392G.
Li, Y., Sun, L., Liu, H., Wang, Y., Liu, Z., 2021. Preparation of single-crystal metal substrates for the growth of high-quality two-dimensional materials. Inorg. Chem. Front. 8, 182–200. https://doi.org/10.1039/d0qi00923g.
Long, D., Liu, S., Zhu, J., Zhang, J., Yuan, X., 2021. Texture and microstructure evolution of ultra-high purity Cu-0.1Al alloy under different rolling methods. Crystals 11, 1113. https://doi.org/10.3390/cryst11091113.
Ma, T., Ariga, H., Takakusagi, S., Asakura, K., 2018. Smooth epitaxial copper film on sapphire surface suitable for high quality graphene growth. Thin Solid Films 646, 12–16. https://doi.org/10.1016/j.tsf.2017.11.009.
Miller, D.L., Keller, M.W., Shaw, J.M., Chiaramonti, A.N., Keller, R.R., 2012. Epitaxial (111) films of Cu, Ni, and Cu_xNi_y on α-Al_2O_3 (0001) for graphene growth by chemical vapor deposition. J. Appl. Phys. 112, 064317. https://doi.org/10.1063/1.4754013.
Nair, R.R., Blake, P., Grigorenko, A.N., Novoselov, K.S., Booth, T.J., Stauber, T., Peres, N. M.R., Geim, A.K., 2008. Fine structure constant defines visual transparency of graphene. Science 320, 1308. https://doi.org/10.1126/science.1156965.
Novoselov, K.S., Geim, A.K., Morozov, S.V., Jiang, D., Zhang, Y., Dubonos, S.V., Grigorieva, I.V., Firsov, A.A., 2004. Electric field effect in atomically thin carbon films. Science 306, 666–669. https://doi.org/10.1126/science.1102896.
Novoselov, K.S., Fal'Ko, V.I., Colombo, L., Gellert, P.R., Schwab, M.G., Kim, K., 2012. A roadmap for graphene. Nature 490, 192–200. https://doi.org/10.1038/nature11458.
Onur, T., Preetha, S., Chang, Q., Matthew, G., Qian, C., Nadya, M., 2024. Tunable magnetic confinement effect in a magnetic superlattice of graphene. npj 2D Mater. Appl. 8, 32. https://doi.org/10.1038/s41699-024-00468-7.
Pang, S., Tsao, H.N., Feng, X., Mullen, K., 2009. Patterned graphene electrodes from solution-processed graphite oxide films for organic field-effect transistors. J. Adv. Mater. 21, 3488–3491. https://doi.org/10.1002/adma.200803812.
Shen, X., Lin, X., Yousefi, N., Jia, J., Kim, J.-K., 2014. Wrinkling in graphene sheets and graphene oxide papers. Carbon 66, 84–92. https://doi.org/10.1016/j.carbon.2013.08.046.
Stoller, M.D., Park, S., Yanwu, Z., An, J., Ruoff, R.S., 2008. Graphene-Based ultracapacitors. Nano Lett. 8, 3498–3502. https://doi.org/10.1021/nl802558y.
Wood, J.D., Schmucker, S.W., Lyons, A.S., Pop, E., Lyding, J.W., 2011. Effects of polycrystalline Cu substrate on graphene growth by chemical vapor deposition. Nano Lett. 11, 4547–4554. https://doi.org/10.1021/nl201566c.
Yang, J., Sardar, B.A., Lei, Y., Emory, C., Haimei, Z., 2019. Dynamic behavior of nanoscale liquids in graphene liquid cells revealed by in situ transmission electron microscopy. Micron 116, 22–29. https://doi.org/10.1016/j.micron.2018.09.009.
Yao, W., Liu, H., Sun, J., Wu, B., Liu, Y., 2022. Engineering of chemical vapor deposition graphene layers: growth, characterization, and properties. Adv. Funct. Mater. 32, 2202584. https://doi.org/10.1002/adfm.202202584.
Zhang, Y., Zhang, L., Zhou, C., 2013. Review of chemical vapor deposition of graphene and related applications. Acc. Chem. Res. 46, 2329–2339. https://doi.org/10.1021/ar300203n.
Yuk, J., Park, J., Ercius, P., Kim, K., Hellebusch, D.J., Crommie, M.F., Lee, J.Y., Zettl, A., Alivisatos, P., 2012. High-resolution EM of colloidal nanocrystal growth using graphene liquid cells. Science 336, 61–64. https://doi.org/10.1126/science.121765.
Zhang, Z., Li, T., 2010. A molecular mechanics study of morphologic interaction between graphene and Si nanowires on a SiO_2 substrate. J. Nanomater. 2011, 374018. https://doi.org/10.1155/2011/374018.
Zheng, L., Liu, N., Gao, X., Zhu, W., Liu, K., Wu, C., Yan, R., Zhang, J., Gao, X., Yao, Y., Deng, B., Xu, J., Lu, Y., Liu, Z., Li, M., Wei, X., Wang, H.-W., Peng, H., 2023. Uniform thin ice on ultraflat graphene for high-resolution cryo-EM. Nat. Methods 20, 123–130. https://doi.org/10.1038/s41592-022-01693-y.